This is the peer-reviewed, final accepted version for American Mineralogist, published by the Mineralogical Society of America.
The published version is subject to change. Cite as Authors (Year) Title. American Mineralogist, in press.
DOI: https://doi.org/10.2138/am-2021-7923. http://www.minsocam.org/

# Evidence from HP/UHP metasediment for recycling of isotopically heterogeneous potassium into the mantle

Ze-Zhou Wang[1, 2*], Fang-Zhen Teng[1*], Vincent Busigny[3, 4], Sheng-Ao Liu[2]

1. Isotope Laboratory, Department of Earth and Space Sciences, University of Washington, Seattle, WA 98195, USA
2. State Key Laboratory of Geological Processes and Mineral Resources, China University of Geosciences, Beijing 100083, China
3. Université de Paris, Institut de Physique du Globe de Paris, CNRS, F-75005, Paris, France
4. Institut Universitaire de France, Paris, France

Abstract: 257 words

Main text: 2688 words

References: 46

Figures: 5

Table: 1

Revised version 1

Submitted to ***American Mineralogist***

February 15, 2020

* Corresponding authors, emails: zzwang74@uw.edu; fteng@uw.edu

This is the peer-reviewed, final accepted version for American Mineralogist, published by the Mineralogical Society of America.
The published version is subject to change. Cite as Authors (Year) Title. American Mineralogist, in press.
DOI: https://doi.org/10.2138/am-2021-7923. http://www.minsocam.org/

## ABSTRACT

Potassium isotopes may provide a novel approach for fingerprinting recycled sediments in the mantle due to the significant differences in K abundance and isotopic ratio between subducting sediment and the mantle. However, the behavior of K isotopes in sediments during subduction zone metamorphism is still unknown. Here we investigate K isotopic composition of a set of well-characterized high- to ultrahigh-pressure metasediments from the Schistes Lustrés nappe (western Alps), which represents marine sediments subducted down to ~90 km depth in a cold subduction zone, and their protoliths from the Lavagna nappe (Apennines, Italy). The metasediments display $\delta^{41}K_{SRM\ 3141a}$ values from -0.76‰ to -0.48‰, which are on average lower than the mantle value (-0.43‰) but similar to those of non-metamorphic equivalents (-0.79‰ to -0.49‰). No systemic variation of $\delta^{41}K$ with metamorphic grade is observed, suggesting negligible K isotope fractionation in these sediments during prograde metamorphism. This is in accord with the limited loss of K during the entire metamorphic history as evidenced by the constancy of K/Rb and K/Cs ratios between metamorphic and non-metamorphic sediments and the absence of correlations of $\delta^{41}K$ with K/Rb and K/Cs. The heterogeneous $\delta^{41}K$ values of metasediments are most likely inherited from their protoliths, which experienced different degree of chemical weathering depending on their provenances. Our results demonstrate that the variable and light K isotopic signatures in subducting sediments could be preserved to depths of at least 90 km along a cold geotherm gradient, indicating that introduction of sediments into the mantle could produce K isotope heterogeneity in the source regions of mantle-derived lavas.

**Keywords:** potassium isotopes; metasediment; metamorphism; subduction zone

## INTRODUCTION

Global subducting sediment (GLOSS) has an average $K_2O$ content (2.21 wt.%; Plank, 2014) several orders of magnitude higher than that of the mantle (0.03 wt.%; McDonough and Sun, 1995). Accordingly, recycling of sediments into the mantle has been commonly invoked to explain the significant K enrichment observed in many mantle-derived lavas such as arc volcanic rocks and EM-type oceanic island basalts (OIBs) relative to mid-ocean ridge basalts (MORBs) (e.g., Plank and Langmuir, 1993; Tatsumi and Eggins, 1995; Elliott, 2003; Jackson and Dasgupta, 2008; Rapp et al., 2008). Recent developments in high-precision K isotope measurements revealed that, compared with the mantle with a mean value of -0.43 defined by global oceanic basalts (Tuller-Ross et al., 2019), subducting sediments display an overall ~1.3‰ variation in $\delta^{41}K$ and commonly have $\delta^{41}K$ values (down to -1.31‰) lower than the mantle (Hu et al., 2020). Low $\delta^{41}K$ value of sediments were mainly ascribed to preferential leaching of heavy K isotopes during chemical weathering (Li et al., 2019a, 2019b; Chen et al., 2020; Hu et al., 2020; Huang et al., 2020; Teng et al., 2020) or incorporation of light K isotopes into authigenic clays during diagenesis (Santiago Ramos et al., 2018; Hu et al., 2020). By contrast, altered oceanic crust (AOC), another major K sink in subducting slabs, has an average $\delta^{41}K$ similar to or higher than the mantle due to interaction with isotopically heavy seawater (Parendo et al., 2017; Hille et al., 2019; Hu et al., 2020; Santiago Ramos et al., 2020). Hence, K isotopes have great potential to discriminate recycled sediments in the mantle. In this regard, the lighter K isotopic compositions relative to the mantle observed in some mantle-derived lavas have been explained to reflect recycled sediments in their mantle sources (e.g. $\delta^{41}K$ down to -0.81‰ for potassic basalts from Northeast China and $\delta^{41}K$ down to -0.60‰ for arc volcanic rocks from Lesser Antilles; Sun et al., 2020; Hu et al., 2021). However, this conclusion relies on the

This is the peer-reviewed, final accepted version for American Mineralogist, published by the Mineralogical Society of America.
The published version is subject to change. Cite as Authors (Year) Title. American Mineralogist, in press.
DOI: https://doi.org/10.2138/am-2021-7923. http://www.minsocam.org/

assumption that K isotopes are not fractionated in sediments during slab subduction into deep mantle, which is still required to be verified.

To date, only one recent study investigated the K isotope behavior during dehydration of subducted oceanic crust. Based on data for eclogites from Tibet, Liu et al. (2020) proposed that dehydration of oceanic crust preferentially releases heavy K isotopes into fluids with an isotope fractionation factor of 1.0015, leaving the residual eclogites extremely enriched in light K isotopes ($\delta^{41}$K down to -1.64‰). Nevertheless, the low-$\delta^{41}$K eclogites are very depleted in K (<0.1 wt.%) and unlikely to be a major isotopically light K input to subduction zones. By contrast, subducting sediments that are highly concentrated in K make up the key isotopically light reservoir within subducting slabs (Plank, 2014; Hu et al., 2020). Moreover, trace elemental studies suggest that "sediment components" dominate the volcanic output of large ion lithophile elements (LILE, e.g., K, Rb, Sr, Ba, Cs) in subduction zones (Plank and Langmuir, 1993). Thus, understanding the behavior of K isotopes in subducting sediments during prograde metamorphism can provide important insights into the fate of sediments in subduction zones particularly on: (1) contribution of sediments to arc magmatism through metamorphic dehydration and/or partial melting and (2) the role of sediments in creating mantle heterogeneity beyond sub-arc regions.

Here we reported K isotopic data for metasediments from the Schistes Lustrés nappe (western Alps) and their protoliths from the Lavagna nappe (northern Apennines, Italy). This suite of samples comprises a continuous metamorphic sequence representative of oceanic sediments subducted at depths between 15 and 90 km along a cold subduction path (Agard et al., 2001; Busigny et al., 2003; Bebout et al., 2013) and thus provides an excellent opportunity to assess element mobility and isotope behavior during forearc devolatilization of sediments.

Previous studies have demonstrated impressive retention of many elements thought to be fluid-mobile (e.g., K, Rb, Cs, Li, B, N, H, C and Cl) and no discernible fractionation of N, H, Li and Cl isotopes in the Schistes Lustrés metasediments across a wide range of metamorphic grade (Busigny et al., 2003; Philippot et al., 2007; Bebout et al., 2013; Cook-Kollars et al., 2014; Barnes et al., 2019; Epstein et al., 2020). We explore the influence of metamorphism on K isotopic compositions of these sediments and evaluate the robustness of K isotopes as a tracer of sediment recycling in the mantle.

## GEOLOGICAL BACKGROUND AND SAMPLES

The western Alps formed following the closure of the approximately north-south trending Valais and Liguro-Piemontese slow-spreading oceans from 100 Ma, through an eastward subduction zone below Apulia/Africa plate at rates of <20 mm/yr (e.g., Rosenbaum and Lister, 2005). The Schistes Lustrés nappe, located in the Piemonte-Ligurian domain of the western Alps (Fig. 1), is mostly composed of upper Mesozoic pelagic metasedimentary rocks that were originally deposited from the Alpine Ocean (e.g., Agard et al., 2009). The peak metamorphic conditions of metasediments from Lago Nero, Fraiteve, Assieta and Finestre continually increase from 0.8 GPa, < 300 $^{o}$C to the west to 1.8-2.0 GPa, 450-500 $^{o}$C to the east (Martin and Polino, 1984; Agard et al., 2001), which is indicated by the successive stability fields of lawsonite, chloritoid and garnet (Agard et al., 2001; Busigny et al., 2003). Samples from Lago di Cignana underwent ultrahigh-pressure (UHP) metamorphism (2.7-2.9 GPa and 630 $^{o}$C; Reinecke, 1998), as exemplified by the occurrence of UHP minerals such as microdiamond and coesite (Reinecke, 1998; Frezzotti et al., 2011). Together, the Schistes Lustrés metasediments represent oceanic sediments that were subducted to variable depths down to ~90 km along a "cold slab" geothermal

This is the peer-reviewed, final accepted version for American Mineralogist, published by the Mineralogical Society of America.
The published version is subject to change. Cite as Authors (Year) Title. American Mineralogist, in press.
DOI: https://doi.org/10.2138/am-2021-7923. http://www.minsocam.org/

93 gradient (~8 $^{o}$C/km).

94 In this study, we measured K isotopic compositions of 12 metasediments from the
95 Schistes Lustrés nappe, covering all the metamorphic grades described above (Busigny et al.,
96 2003). They mainly consist of quartz, carbonate, phengite, paragonite and chlorite with minor
97 amounts of lawsonite, garnet, rutile, graphite and/or epidote (Busigny et al., 2003). The
98 lithologies range from calc-schist to siliceous metapelite depending on the modal abundance of
99 carbonate (0-49%). The petrology, major-trace element and C-H-O-N isotope geochemistry of
100 these samples have been reported in Busigny et al. (2003), which found large variations in $K_2O$
101 content (0.61-7.96 wt.%). For comparison, we also analyzed four non-metamorphic sediments
102 from the Lavagna nappe lying within the internal Ligurid units of the Northern Apennines, Italy
103 (Fig. 1), which were taken as protoliths of the Schistes Lustrés metasediments (Busigny et al.,
104 2003). These samples include marls, calcareous and siliceous pelites, with variable proportions
105 of calcite, clay minerals (mostly illite) and quartz, and experienced low-grade diagenetic
106 alteration ($P$ < 0.17 GPa and $T$ < 300 $^{o}$C) (Bonazzi et al., 1987; Reinhardt, 1991). Their $K_2O$
107 contents vary from 1.20 to 4.75 wt.% (Fig. 2).
108

109 **METHODS**

110 Potassium isotopic analyses were carried out at the Isotope Laboratory of the University
111 of Washington, Seattle, following a protocol reported in Hu et al. (2018) and Xu et al. (2019).
112 Only a brief description is provided below. Approximately 10-15 mg whole-rock powders were
113 dissolved in a mixture of Optima-grade HF-$HNO_3$-HCl to achieve complete dissolution.
114 Afterwards, the solutions were evaporated to dryness and redissolved in 0.5N $HNO_3$. Sample
115 solution in 1 ml 0.5 N $HNO_3$ was loaded onto a column filled with 2 ml Bio-Rad AG 50W-X8

cation exchange resin (200-400 mesh) to separate K from other matrix elements. The column chromatographic procedure was performed twice with the K yield approaching 100% and the total procedural K blank < 9 ng.

The K isotopic ratios were measured on a Nu Plasma II multicollector inductively coupled plasma mass spectrometer. To minimize the isobaric interference of $ArH^+$ on $^{41}K^+$, sample solution in 3% $HNO_3$ was introduced into a "cold plasma" via a CETAC Aridus II desolvating nebulizer system at the RF power of 700 W. The signals of $^{39}K^+$ and $^{41}K^+$ were measured simultaneously at the interference-free shoulder using pseudo-high resolution mode. Around 4-6 V signal of $^{39}K^+$ can be obtained for solutions containing 3 ppm of K. Instrumental mass bias was corrected using standard-sample bracketing method. The final results are reported in δ notation against the K standard NIST SRM 3141a:

$$\delta^{41}K\ (‰) = \left\{ \frac{\left(^{41}K/^{39}K\right)_{sample}}{\left(^{41}K/^{39}K\right)_{SRM\ 3141a}} - 1 \right\} \times 1000$$

A long-term external precision better than 0.06‰ (95% confidential interval) is routinely achieved based on repeated analysis of geostandards and pure K solutions (Hu et al., 2018). A shale standard SCo-1 and a granite standard G-2 analyzed in the course of this study yielded $\delta^{41}K$ values of -0.40 ± 0.04‰ and -0.46 ± 0.05‰ (Table 1), respectively, which are in good agreement with the results reported previously (Chen et al., 2019; Li et al., 2019b; Xu et al., 2019).

## RESULTS

The K isotopic compositions of all samples investigated in this study are reported in Table 1. The Schistes Lustrés metasediments have $\delta^{41}K$ values from -0.76 ± 0.04‰ to -0.48 ±

137 0.03‰, averaging at -0.61 ± 0.15‰ (2SD, n = 12). No systematic variation in $\delta^{41}K$ is observed
138 with increasing metamorphic grade (Fig. 2). The Lavagna non-metamorphic rocks display a
139 similar range in $\delta^{41}K$ from -0.79 ± 0.04‰ to -0.49 ± 0.04‰, with a mean of -0.58 ± 0.28‰
140 (2SD, n = 4). Notably, most samples have K isotopic compositions lighter than the average
141 mantle ($\delta^{41}K$ = -0.43‰; Tuller-Ross et al., 2019) and upper continental crust ($\delta^{41}K$ = -0.44‰;
142 Huang et al., 2020). Such light K isotopic signatures have also been observed in sediments or
143 sedimentary rocks reported previously ($\delta^{41}K$ = -1.31‰ to -0.02‰; Li et al., 2019a, 2019b; Chen
144 et al., 2020; Hu et al., 2020; Huang et al., 2020; Teng et al., 2020).
145
146 **DISCUSSION**
147 The significant K isotopic variation in metasediments might reflect isotope fractionation
148 during metamorphism, protolith heterogeneity or both. Below, we first examine the effects of
149 metamorphism and protolith heterogeneity on the observed K isotopic variation, then discuss the
150 implications for K isotope geochemistry of arc magmatism and mantle heterogeneity.
151
152 **Metamorphism**
153 The K budget in the Schistes Lustrés metasediments is dominated by phengite, with
154 minor K hosted in paragonite (Bebout et al., 2013), which is depicted by the whole rock data
155 falling along a linear trend between bulk $K_2O$ content and $K_2O/(SiO_2 + Al_2O_3)$ defined by the
156 phengite and paragonite (Fig. 3). Further support for the whole-rock $K_2O$ variations resulting
157 from variable abundance of phengite in metasediments comes from the positive relationship
158 between $K_2O$ and $H_2O$ (Fig. 4a). Therefore, the behaviors of K and its isotopes in metapelites
159 during metamorphism are strictly controlled by metamorphic reactions involving phengite as it is

This is the peer-reviewed, final accepted version for American Mineralogist, published by the Mineralogical Society of America.
The published version is subject to change. Cite as Authors (Year) Title. American Mineralogist, in press.
DOI: https://doi.org/10.2138/am-2021-7923. http://www.minsocam.org/

the main K host in our samples. Phengite breakdown will release $H_2O$ and K into fluids, resulting in a decrease in $H_2O$ and $K_2O$ contents of the residual metasediments. However, $H_2O$ and $K_2O$ are not depleted in the majority of metasediments compared with their purported protoliths and their contents do not correlate with metamorphic grade either (Figs. 2, 4a), indicating limited breakdown of phengite and K loss during metamorphism.

To eliminate the potential impact of protolith heterogeneity on $K_2O$ content, we employed $K_2O$/Rb and $K_2O$/Cs ratios as indicators of K loss. Because of the similar ionic radius among K, Rb and Cs, Rb and Cs are partitioned predominantly into K-bearing minerals (i.e., phengite in this study). Consequently, the $K_2O$/Rb and $K_2O$/Cs ratios of whole-rock reflect those of phengite. Based on this assumption, the extent of phengite breakdown ($F$) in an open system can be calculated through the Rayleigh distillation equation: $R^0 = R^1 \times (1\text{-}F)^{(\frac{1}{K_D}\text{-}1)}$ (Busigny et al., 2003), where $R^0$ and $R^1$ represent the $K_2O$/Rb and $K_2O$/Cs ratios in phengite before and after dehydration, respectively, and $K_D$ refers to the Rb-K or Cs-K exchange coefficient between phengite and fluid. Using this method and the exchange coefficient determined by Melzer and Wunder (2000), Busigny et al. (2003) found that strong fractionation between K and Rb or Cs could be induced by a small degree of phengite dehydration (indicated by the dashed curves in Figs. 4b-c). However, almost all samples including metamorphic and non-metamorphic sediments display linear trends in the $K_2O$ vs. Rb and $K_2O$ vs. Cs diagrams and the maximum extent of phengite breakdown is below 5%. The above observations, together with previous studies of other fluid-mobile and volatile element systems (e.g., Ba, Li, B, N, H, C and Cl; Busigny et al., 2003; Philippot et al., 2007; Bebout et al., 2013; Cook-Kollars et al., 2014; Barnes et al., 2019; Epstein et al., 2020), strongly suggest that the Schistes Lustrés metasediments remained almost in closed systems at the bulk-rock scale during the entire metamorphic history.

This is the peer-reviewed, final accepted version for American Mineralogist, published by the Mineralogical Society of America.
The published version is subject to change. Cite as Authors (Year) Title. American Mineralogist, in press.
DOI: https://doi.org/10.2138/am-2021-7923. http://www.minsocam.org/

Therefore, metamorphic overprinting of K isotopic systems in these metasediments is minimal, which is also evidenced by the same overall range in $\delta^{41}K$ as their protoliths (Fig. 2) and the lack of obvious correlations of $\delta^{41}K$ with $H_2O$, $K_2O/Rb$ and $K_2O/Cs$ (Figs. 4d-f).

**Protolith heterogeneity**

Both metamorphic and non-metamorphic samples studied here cover a range of lithologies from carbonate-rich to silicate-rich pelites (Busigny et al., 2003). The heterogeneous protoliths are likely responsible for the variation in K isotopic compositions of the Schistes Lustrés metasediments. This is particularly well illustrated by the most siliceous metamorphic sample (7-00), which has the lowest $\delta^{41}K$ value close to the most siliceous unmetamorphosed equivalent (00-Li7) (Fig. 5a).

Despite the lithological variation, recent studies revealed that varying intensity of chemical weathering exerts a fundamental control on producing the large $\delta^{41}K$ range of sediments (Li et al., 2019a, 2019b; Chen et al., 2020; Huang et al., 2020; Teng et al., 2020). During chemical weathering, heavy K isotopes are preferentially leached by fluids, as demonstrated by the high $\delta^{41}K$ values of river water and seawater (Hille et al., 2019; Li et al., 2019a; Teng et al., 2020; Wang et al., 2020, 2021). Correspondingly, the $\delta^{41}K$ values of weathered residues are shifted towards lower values with increasing intensity of weathering (Chen et al., 2020; Teng et al., 2020). Therefore, sediments sourced from highly weathered provenances often have low $\delta^{41}K$ values.

All metasediments in this study have very high chemical index of alteration values (CIA, defined in the footnote of Table 1) from 69 to 85, resembling those of the Lavagna unmetamorphosed sediments (73-83). Their $\delta^{41}K$ values overlap with those of sediments

206 reported previously at similar CIA values (Fig. 5b). Although there is no correlation between
207 CIA and $\delta^{41}K$ due to the narrow range of CIA and/or protolith heterogeneity, the variable and
208 low $\delta^{41}K$ values of these metasediments likely inherited the signatures from surface weathering
209 of their protoliths. This hypothesis is supported by the low Li isotopic ratios, a typical feature of
210 weathered sediments (e.g., Penniston-Dorland et al., 2017), observed in the Schistes Lustrés
211 metasediments with high CIA values similar to those of our samples (Barnes et al., 2019).
212

213 **IMPLICATIONS**

214 The absence of K isotope fractionation during prograde metamorphism documented in
215 the Schistes Lustrés metasediments confirms that the variable K isotopic compositions of
216 subducting sediments can be preserved to depths at least approaching those beneath volcanic
217 fronts (~90 km) along a cold geotherm gradient typical for most modern subduction zones.
218 Nevertheless, it remains unclear whether K isotopes are fractionated in sediments during warmer
219 subduction. Experimental studies showed that aqueous fluids derived from slab dehydration even
220 under P-T conditions of warm subduction zones contain limited amount of K (Johnson and
221 Plank, 2000; Hermann and Spandler, 2008). Thus, limited K isotope fractionation induced by
222 sediment dehydration along a hot subduction path may also be expected. The light K isotopic
223 signatures of metasediments are distinct from the speculative $^{41}K$-enriched fluids released
224 through dehydration of oceanic mafic crust (Liu et al., 2020). This makes K isotopes an effective
225 tool to distinguish recycled sediments from fluids in the petrogenesis of arc magmas, as
226 illustrated in studies of the Lesser Antilles arc lavas (Hu et al., 2021). Furthermore, sediments
227 may survive from dehydration melting and transport substantial K into deeper mantle beyond
228 sub-arc depths (Hermann and Spandler, 2008; Rapp et al., 2008; Grassi and Schmidt, 2011).

Indeed, two studies on deep mantle-derived lavas have revealed low $\delta^{41}K$ values in EM1-type intracontinental potassic basalts from northeast China (as low as -0.81‰; Sun et al., 2020) and some EM2-type OIBs from Society hotspot (as low as -0.57‰; Tuller-Ross et al., 2019), both of which might manifest the recycling of sediments into the mantle transition zone and even lower mantle.

## ACKNOWLEDGEMENTS AND FUNDING

We dedicated this paper to Prof. John Valley, who has inspired us in many fields, in particular in stable isotope geochemistry and metamorphic petrology. We are grateful to Xin-Yang Chen, Yan Hu, Tian-Yi Huang and Kai-Chen Xing for their help during K isotopic analysis. This manuscript benefited from insightful comments from Dr. Danielle Santiago Ramos and one anonymous reviewer. The careful and efficient editorial handing by Dr. William Peck is highly appreciated. We acknowledge the financial support from the National Key R&D Program of China (2019YFA0708402) to S.-A.L and the Institut Universitaire de France (IUF#2017-2021) to V.B.

## REFERENCES CITED

Agard, P., Vidal, O., and Goffé, B. (2001) Interlayer and Si content of phengite in HP-LT carpholite-bearing metapelites. Journal of Metamorphic Geology, 19, 479-495.

Agard, P., Yamato, P., Jolivet, L., and Burov, E. (2009) Exhumation of oceanic blueschists and eclogites in subduction zones: timing and mechanisms. Earth-Science Reviews, 92, 53-79.

Barnes, J.D., Penniston-Dorland, S.C., Bebout, G.E., Hoover, W., Beaudoin, G.M., and Agard, P. (2019) Chlorine and lithium behavior in metasedimentary rocks during prograde

253 metamorphism: A comparative study of exhumed subduction complexes (Catalina Schist
254 and Schistes Lustrés). Lithos, 336, 40-53.
255 Bebout, G.E., Agard, P., Kobayashi, K., Moriguti, T., and Nakamura, E. (2013) Devolatilization
256 history and trace element mobility in deeply subducted sedimentary rocks: Evidence from
257 Western Alps HP/UHP suites. Chemical Geology, 342, 1-20.
258 Bonazzi, A., Cortesogno, L., Galbiati, B., Reinhardt, M., and Salvioli Mariani, E. (1987) Nuovi
259 dati sul metamorfismo di basso grado nelle unità liguridi interne e loro possibile
260 significato nell'evoluzione strutturale dell'Appennino settentrionale. Acta naturalia de
261 l'Ateneo parmense, 23, 17-47.
262 Busigny, V., Cartigny, P., Philippot, P., Ader, M., and Javoy, M. (2003) Massive recycling of
263 nitrogen and other fluid-mobile elements (K, Rb, Cs, H) in a cold slab environment:
264 evidence from HP to UHP oceanic metasediments of the Schistes Lustrés nappe (western
265 Alps, Europe). Earth and Planetary Science Letters, 215, 27-42.
266 Chen, H., Tian, Z., Tuller-Ross, B., Korotev, R.L., and Wang, K. (2019) High-precision
267 potassium isotopic analysis by MC-ICP-MS: an inter-laboratory comparison and refined
268 K atomic weight. Journal of Analytical Atomic Spectrometry, 34, 160-171.
269 Chen, H., Liu, X.-M., and Wang, K. (2020) Potassium isotope fractionation during chemical
270 weathering of basalts. Earth and Planetary Science Letters, 539, 116192.
271 Cook-Kollars, J., Bebout, G.E., Collins, N.C., Angiboust, S., and Agard, P. (2014) Subduction
272 zone metamorphic pathway for deep carbon cycling: I. Evidence from HP/UHP
273 metasedimentary rocks, Italian Alps. Chemical Geology, 386, 31-48.
274 Elliott, T. (2003) Tracers of the slab, Inside the Subduction Factory. Geophysical Monograph-
275 American Geophysical Union, pp. 23-46.

276 Epstein, G.S., Bebout, G.E., Angiboust, S., and Agard, P. (2020) Scales of fluid-rock interaction
277 and carbon mobility in the deeply underplated and HP-Metamorphosed Schistes Lustrés,
278 Western Alps. Lithos, 354, 354-355.
279 Frezzotti, M., Selverstone, J., Sharp, Z., and Compagnoni, R. (2011) Carbonate dissolution
280 during subduction revealed by diamond-bearing rocks from the Alps. Nature Geoscience,
281 4, 703-706.
282 Grassi, D., and Schmidt, M.W. (2011) The melting of carbonated pelites from 70 to 700 km
283 depth. Journal of Petrology, 52, 765-789.
284 Hermann, J., and Spandler, C.J. (2008) Sediment melts at sub-arc depths: an experimental study.
285 Journal of Petrology, 49, 717-740.
286 Hille, M., Hu, Y., Huang, T.-Y., and Teng, F.-Z. (2019) Homogeneous and heavy potassium
287 isotopic composition of global oceans. Science Bulletin, 64, 1740-1742.
288 Hu, Y., Chen, X.-Y., Xu, Y.-K., and Teng, F.-Z. (2018) High-precision analysis of potassium
289 isotopes by HR-MC-ICPMS. Chemical Geology, 493, 100-108.
290 Hu, Y., Teng, F.-Z., Plank, T., and Chauvel, C. (2020) Potassium isotopic heterogeneity in
291 subducting oceanic plates. Science Advances, 6, eabb2472.
292 Hu, Y., Teng, F.-Z., and Chauvel, C. (2021) Potassium isotopic evidence for sedimentary input to
293 the mantle source of Lesser Antilles lavas. Geochimica et Cosmochimica Acta, 295, 98-
294 111.
295 Huang, T.-Y., Teng, F.-Z., Rudnick, R.L., Chen, X.-Y., Hu, Y., Liu, Y.-S., and Wu, F.-Y. (2020)
296 Heterogeneous potassium isotopic composition of the upper continental crust.
297 Geochimica et Cosmochimica Acta, 278, 122-136.
298 Jackson, M.G., and Dasgupta, R. (2008) Compositions of HIMU, EM1, and EM2 from global

299 trends between radiogenic isotopes and major elements in ocean island basalts. Earth
300 Planetary Science Letters, 276, 175-186.
301 Johnson, M.C., and Plank, T. (2000) Dehydration and melting experiments constrain the fate of
302 subducted sediments. Geochemistry, Geophysics, Geosystems, 1, 1-26.
303 Li, S., Li, W., Beard, B.L., Raymo, M.E., Wang, X., Chen, Y., and Chen, J. (2019a) K isotopes as
304 a tracer for continental weathering and geological K cycling. Proceedings of the National
305 Academy of Sciences, 116, 8740-8745.
306 Li, W., Li, S., and Beard, B.L. (2019b) Geological cycling of potassium and the K isotopic
307 response: insights from loess and shales. Acta Geochimica, 38, 508-516.
308 Liu, H., Wang, K., Sun, W.-D., Xiao, Y., Xue, Y.-Y., and Tuller-Ross, B. (2020) Extremely light
309 K in subducted low-T altered oceanic crust: Implications for K recycling in subduction
310 zone. Geochimica et Cosmochimica Acta, 277, 206-223.
311 Martin, S., and Polino, R. (1984) Le metaradiolariti a ferro di Cesana (Valle di Susa-Alpi
312 occidentali). Mem. Soc. Geol. It, 29, 107-125.
313 McDonough, W.F., and Sun, S.-S. (1995) The composition of the Earth. Chemical Geology, 120,
314 223-253.
315 Melzer, S., and Wunder, B. (2000) Island-arc basalt alkali ratios: Constraints from phengite-fluid
316 partitioning experiments. Geology, 28, 583-586.
317 Parendo, C.A., Jacobsen, S.B., and Wang, K. (2017) K isotopes as a tracer of seafloor
318 hydrothermal alteration. Proceedings of the National Academy of Sciences, 114, 1827.
319 Penniston-Dorland, S., Liu, X.-M., and Rudnick, R.L. (2017) Lithium isotope geochemistry.
320 Reviews in Mineralogy and Geochemistry, 82, 165-217.
321 Philippot, P., Busigny, V., Scambelluri, M., and Cartigny, P. (2007) Oxygen and nitrogen isotopes

as tracers of fluid activities in serpentinites and metasediments during subduction. Mineralogy and Petrology, 91, 11-24.

Plank, T., and Langmuir, C.H. (1993) Tracing trace elements from sediment input to volcanic output at subduction zones. Nature, 362, 739-743.

Plank, T. (2014) The chemical composition of subducting sediments, Treatise on Geochemistry (Second Edition). Elsevier, Oxford, pp. 607-629.

Rapp, R.P., Irifune, T., Shimizu, N., Nishiyama, N., Norman, M.D., and Inoue, T. (2008) Subduction recycling of continental sediments and the origin of geochemically enriched reservoirs in the deep mantle. Earth and Planetary Science Letters, 271, 14-23.

Reinecke, T. (1998) Prograde high-to ultrahigh-pressure metamorphism and exhumation of oceanic sediments at Lago di Cignana, Zermatt-Saas Zone, western Alps. Lithos, 42, 147-189.

Reinhardt, M. (1991) Vitrinite reflectance, illite crystallinity and tectonics: results from the Northern Apennines (Italy). Organic geochemistry, 17, 175-184.

Rosenbaum, G., and Lister, G.S. (2005) The Western Alps from the Jurassic to Oligocene: spatio-temporal constraints and evolutionary reconstructions. Earth-Science Reviews, 69, 281-306.

Rudnick, R., and Gao, S. (2014) Composition of the continental crust, Treatise on Geochemistry (Second Edition). Elsevier, Oxford, pp. 1-51.

Santiago Ramos, D.P., Morgan, L.E., Lloyd, N.S., and Higgins, J.A. (2018) Reverse weathering in marine sediments and the geochemical cycle of potassium in seawater: Insights from the K isotopic composition (41K/39K) of deep-sea pore-fluids. Geochimica et Cosmochimica Acta, 236, 99-120.

345 Santiago Ramos, D.P., Coogan, L.A., Murphy, J.G., and Higgins, J.A. (2020) Low-temperature
346 oceanic crust alteration and the isotopic budgets of potassium and magnesium in
347 seawater. Earth and Planetary Science Letters, 541, 116290.
348 Sun, Y., Teng, F.-Z., Hu, Y., Chen, X.-Y., and Pang, K.-N. (2020) Tracing subducted oceanic
349 slabs in the mantle by using potassium isotopes. Geochimica et Cosmochimica Acta, 278,
350 353-360.
351 Tatsumi, Y., and Eggins, S. (1995) Subduction zone magmatism. Wiley.
352 Teng, F.-Z., Hu, Y., Ma, J.-L., Wei, G.-J., and Rudnick, R.L. (2020) Potassium isotope
353 fractionation during continental weathering and implications for global K isotopic
354 balance. Geochimica et Cosmochimica Acta, 278, 261-271.
355 Tuller-Ross, B., Marty, B., Chen, H., Kelley, K.A., Lee, H., and Wang, K. (2019) Potassium
356 isotope systematics of oceanic basalts. Geochimica et Cosmochimica Acta, 259, 144-154.
357 Wang, K., Close, H.G., Tuller-Ross, B., and Chen, H. (2020) Global average potassium isotope
358 composition of modern seawater. ACS Earth and Space Chemistry, 4, 1010-1017.
359 Wang, K., Peucker-Ehrenbrink, B., Chen, H., Lee, H., and Hasenmueller, E.A. (2021) Dissolved
360 potassium isotopic composition of major world rivers. Geochimica et Cosmochimica
361 Acta, 294, 145-159.
362 Workman, R.K., and Hart, S.R. (2005) Major and trace element composition of the depleted
363 MORB mantle (DMM). Earth and Planetary Science Letters, 231, 53-72.
364 Xu, Y.-K., Hu, Y., Chen, X.-Y., Huang, T.-Y., Sletten, R.S., Zhu, D., and Teng, F.-Z. (2019)
365 Potassium isotopic compositions of international geological reference materials.
366 Chemical Geology, 513, 101-107.
367

This is the peer-reviewed, final accepted version for American Mineralogist, published by the Mineralogical Society of America.
The published version is subject to change. Cite as Authors (Year) Title. American Mineralogist, in press.
DOI: https://doi.org/10.2138/am-2021-7923. http://www.minsocam.org/

368 **FIGURE CAPTIONS**

369 **Figure 1.** Sketch tectonic map of the western Alps and northern Apennines (modified after
370 Busigny et al., 2003). From south to north, internal crystalline massifs are Dora Maira, Grand
371 Paradiso and Monte Rosa, respectively. The peak *P-T* condition of each sampling zone is from
372 Busigny et al. (2003).

373

374 **Figure 2.** Variations of $K_2O$ and $\delta^{41}K$ with increasing metamorphic grade. Symbols with
375 different colors refer to different metamorphic grades. The grey horizontal bar represents the
376 average $\delta^{41}K$ value of samples of each grade and the grey band refers to the 2SE range.

377

378 **Figure 3.** Variation of $K_2O$ with $K_2O/(SiO_2+Al_2O_3)$ (symbols as in Fig. 3). The original data are
379 from Busigny et al. (2003) and reported in Table 1. Data for the Schistes Lustrés metasediments
380 (open diamonds) reported in Bebout et al. (2013) and Epstein et al. (2020) are also shown for
381 comparison. Data for phengites and paragonites in the Schistes Lustrés metasediments are from
382 Bebout et al. (2013). The black line refers to the least square line of best fit throughout all the
383 studied samples.

384

385 **Figure 4.** Plots of (a) $K_2O$ versus $H_2O$, (b) $K_2O$ versus Rb, (c) $K_2O$ versus Cs, (d) $\delta^{41}K$ versus
386 $H_2O$, (e) $\delta^{41}K$ versus $K_2O$/Rb, and (f) $\delta^{41}K$ versus $K_2O$/Cs (symbols as in Fig. 3). Open diamonds
387 in (b) and (c) are the Schistes Lustrés metasediments from Bebout et al. (2013) and Epstein et al.
388 (2020). Data for phengites are from Bebout et al. (2013). The black lines in (b) and (c) are the
389 least square lines of best fit throughout the studied metasediments. The dashed curves in (b) and
390 (c) refer to the variations in $K_2O$, Rb and Cs concentrations of metasediments during

391 devolatilization, which are simulated using the same methods and parameters as those reported in
392 Busigny et al. (2003). Numbers next to small black circles indicate the fraction of phengite
393 broken down.
394
395 **Figure 5.** Plots of (a) $\delta^{41}K$ versus $SiO_2$ and (b) $\delta^{41}K$ versus CIA (chemical index of alteration, see
396 definition in footnote of Table 1) (symbols as in Fig. 3). The grey squares represent sediments or
397 sedimentary rocks reported in literature (Li et al., 2019a, 2019b; Chen et al., 2020; Hu et al.,
398 2020; Huang et al., 2020; Teng et al., 2020). The average CIA (50.76) and $\delta^{41}K$ value (-0.44‰)
399 of upper continental crust are from Rudnick and Gao (2014) and Huang et al. (2020),
400 respectively.

This is the peer-reviewed, final accepted version for American Mineralogist, published by the Mineralogical Society of America.
The published version is subject to change. Cite as Authors (Year) Title. American Mineralogist, in press.
DOI: https://doi.org/10.2138/am-2021-7923. http://www.minsocam.org/

**Table 1** Potassium isotopic compositions of the Lavagna sediments, the Schistes Lustrés metasediments and geostandards, together with selected major and trace elemental data.

| Sample | $SiO_2$ (wt.%) | $Al_2O_3$ (wt.%) | $CaCO_3$ (wt.%) | $K_2O$ (wt.%) | $Na_2O$ (wt.%) | CaO (wt.%) | $H_2O$ (wt.%) | Rb (ppm) | Cs (ppm) | CIA | $\delta^{41}K$ (‰) | 2SD (‰) | 95% c.i. (‰) | N |
|---|---|---|---|---|---|---|---|---|---|---|---|---|---|---|
| ***Lavagna (unmetamorphosed)*** | | | | | | | | | | | | | | |
| 00Li10 | 40.98 | 16.66 | 17 | 2.44 | 0.66 | 11.49 | 4.82 | 117 | 6.4 | 82 | -0.51 | 0.06 | 0.04 | 7 |
| 00Li8S | 58.99 | 20.58 | 1 | 4.75 | 1.36 | 0.85 | 4.10 | 229 | 15.6 | 74 | -0.54 | 0.04 | 0.04 | 7 |
| 00Li9 | 22.91 | 7.90 | 68 | 1.20 | 0.16 | 32.06 | 3.20 | 62 | 3.8 | 83 | -0.49 | 0.07 | 0.04 | 7 |
| 00-Li7 | 79.10 | 8.90 | 0 | 2.22 | 0.53 | 0.20 | 2.08 | 97 | 6.1 | 73 | -0.79 | 0.04 | 0.04 | 7 |
| ***Lago Nero (0.8 GPa/300 ºC)*** | | | | | | | | | | | | | | |
| C18 | 62.00 | 8.28 | 13 | 0.93 | 0.72 | 11.34 | 2.00 | 51 | 3.2 | 79 | -0.56 | 0.07 | 0.04 | 13 |
| ***Fraiteve (1.5 GPa/350 ºC)*** | | | | | | | | | | | | | | |
| 98SE3 | 38.41 | 11.33 | 19 | 1.36 | 0.31 | 19.56 | 4.36 | 72 | 4.4 | 85 | -0.68 | 0.08 | 0.04 | 7 |
| SL98-2P | 54.49 | 19.80 | 2 | 2.48 | 0.48 | 4.99 | 5.96 | 126 | 7.4 | 85 | -0.61 | 0.08 | 0.03 | 14 |
| ***Assieta (1.8 GPa/400 ºC)*** | | | | | | | | | | | | | | |
| 98SE5 | 48.71 | 27.67 | 0 | 7.07 | 0.33 | 0.00 | 5.19 | 341 | 19.6 | 77 | -0.48 | 0.08 | 0.03 | 7 |
| 98SE6 | 45.54 | 28.02 | 0 | 5.23 | 1.58 | 0.18 | 5.78 | 272 | 16.0 | 77 | -0.57 | 0.06 | 0.03 | 7 |
| SL98-3C | 29.13 | 7.56 | 49 | 0.88 | 0.50 | 30.89 | 2.78 | 45 | 2.4 | 81 | -0.52 | 0.06 | 0.03 | 7 |
| SL98-3P | 46.43 | 28.30 | 0 | 7.96 | 0.19 | 0.22 | 5.44 | 347 | 19.7 | 76 | -0.63 | 0.04 | 0.03 | 7 |
| ***Finestre (2.0 GPa/450 ºC)*** | | | | | | | | | | | | | | |
| 98SE7 | 39.80 | 4.04 | 44 | 0.61 | 0.19 | 29.13 | 1.24 | 39 | 2.4 | 81 | -0.60 | 0.05 | 0.03 | 7 |
| 98SE8 | 68.06 | 13.24 | 2 | 3.52 | 0.17 | 1.93 | 2.80 | 151 | 9.0 | 76 | -0.65 | 0.03 | 0.03 | 7 |
| 98SE9 | 43.75 | 17.54 | 21 | 2.94 | 0.64 | 12.27 | 3.88 | 127 | 7.3 | 81 | -0.65 | 0.06 | 0.03 | 7 |
| ***Lago di Cignana (2.9 GPa/630 ºC)*** | | | | | | | | | | | | | | |
| 90-25A | 43.52 | 10.81 | 29 | 2.23 | 0.49 | 18.01 | 2.45 | 109 | 4.9 | 77 | -0.63 | 0.04 | 0.04 | 7 |
| 7-00 | 79.79 | 8.80 | 0 | 2.08 | 0.99 | 0.54 | 1.16 | 94 | 5.9 | 69 | -0.76 | 0.07 | 0.04 | 7 |
| ***Geostandards*** | | | | | | | | | | | | | | |
| SCo-1 | | | | | | | | | | | -0.40 | 0.07 | 0.04 | 11 |
| G-2 | | | | | | | | | | | -0.46 | 0.09 | 0.05 | 12 |

Note: Major and trace elemental data are from Busigny et al. (2003), except for $Al_2O_3$, $Na_2O$, and CaO, which are reported here for the first time and were determined by ICP-AES following the same method described in Busigny et al. (2003). CIA = molar ratio of $100*Al_2O_3/(Al_2O_3+Na_2O+K_2O+CaO^*)$, where CaO* refers to the CaO content of silicate fraction only (Nesbitt and Young, 1982). 2SD refers to two standard deviation. 95% c.i. is 95% confidential interval, which is calculated using the equation of $t\frac{SD}{\sqrt{N}}$, where $t$ is the Student's t factor and N refers to number of measurements (see details in Hu et al., 2018a).

This is the peer-reviewed, final accepted version for American Mineralogist, published by the Mineralogical Society of America.
The published version is subject to change. Cite as Authors (Year) Title. American Mineralogist, in press.
DOI: https://doi.org/10.2138/am-2021-7923. http://www.minsocam.org/

# Figure 1

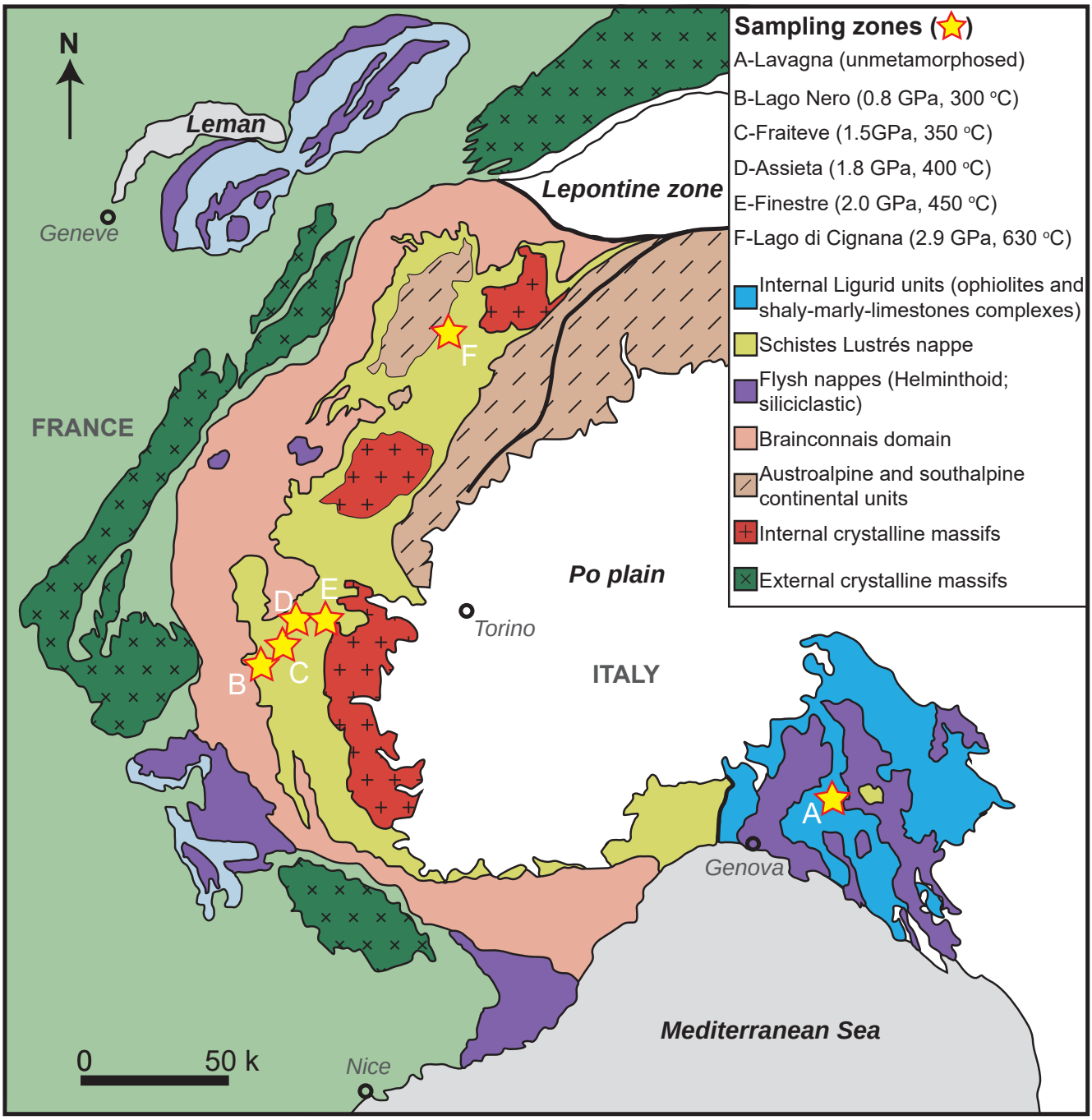

# Figure 2

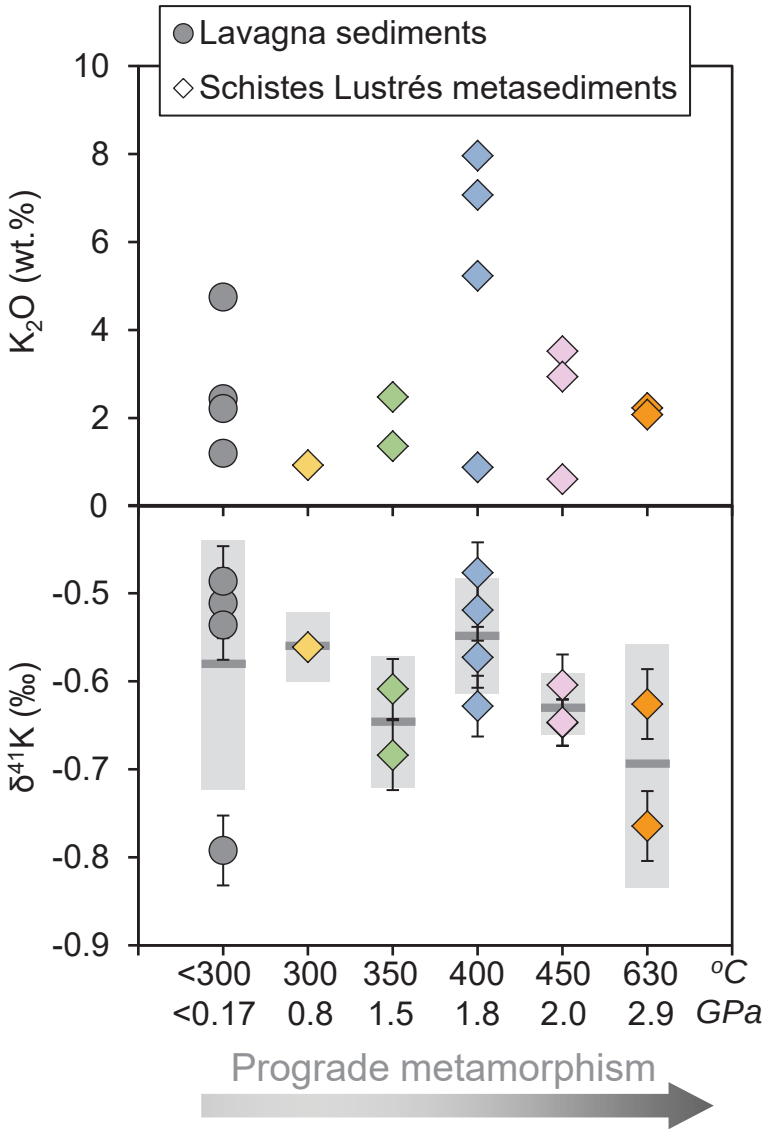

This is the peer-reviewed, final accepted version for American Mineralogist, published by the Mineralogical Society of America.
The published version is subject to change. Cite as Authors (Year) Title. American Mineralogist, in press.
DOI: https://doi.org/10.2138/am-2021-7923. http://www.minsocam.org/

# Figure 3

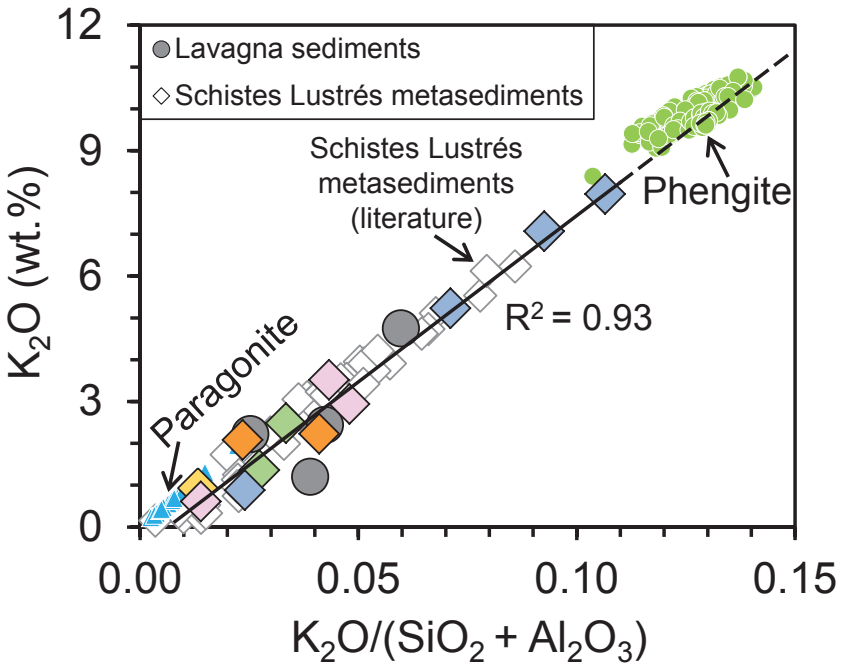

This is the peer-reviewed, final accepted version for American Mineralogist, published by the Mineralogical Society of America.
The published version is subject to change. Cite as Authors (Year) Title. American Mineralogist, in press.
DOI: https://doi.org/10.2138/am-2021-7923. http://www.minsocam.org/

# Figure 4

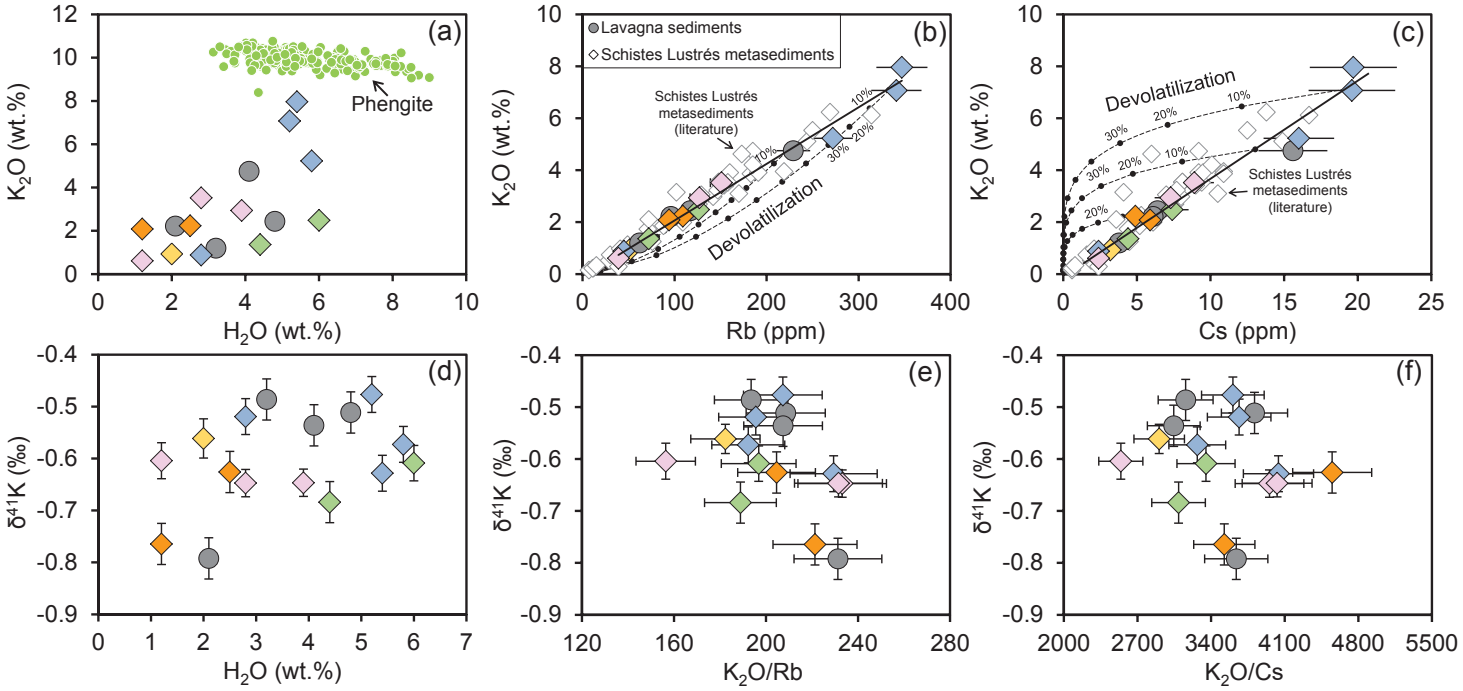

# Figure 5